

# Ultra-cold Collisions between Spin-Orbit-Coupled Dipoles: General Formalism and Universality

Jia Wang, Christiaan R. Hougaard, Brendan C. Mulkerin, and Xia-Ji Liu

Centre for Quantum and Optical Science, Swinburne University of Technology, Melbourne 3122, Australia

(Dated: May 18, 2021)

A theoretical study of the low-energy scattering properties of two aligned identical bosonic and fermionic dipoles in the presence of isotropic spin-orbit coupling (SOC) is presented. A general treatment of particles with arbitrary (pseudo-) spin is given in the framework of multi-channel scattering. At ultracold temperatures and away from shape resonances or closed-channel dominated resonances, the cross-section can be well described within the Born approximation to within corrections due to the  $s$ -wave scattering. We compare our findings with numerical calculations and find excellent agreement.

## I. INTRODUCTION

Many novel behaviors and phases in quantum few- and many-body systems can be understood from the competition between kinetic and interaction energies. The extraordinary degree of control in systems of ultracold quantum gases, therefore, provides versatile platforms to study these quantum phenomena [1–4]. For instance, short-range interactions (or more precisely,  $s$ -wave scattering lengths) between atoms can be tuned to virtually arbitrary values via magnetic Feshbach resonances [5], allowing us to access the unitary regime [6–8] and study Efimov physics [9–11]. On the other hand, long-range interactions, especially the anisotropic dipole-dipole interactions, can significantly change the excitation spectrum [12] and the stability diagrams of Bose-Einstein Condensation (BEC) [13–15], which has attracted intense interest in gases of ultracold heteronuclear ground state molecules [16, 17], and magnetic dipolar atoms such as  $^{52}\text{Cr}$  [14],  $^{164}\text{Dy}$  [18, 19], and  $^{168}\text{Er}$  [20]. More recently, manipulating kinetic energies and corresponding dispersion relationship has been realized via the innovative synthetic spin-orbit coupling (SOC) technique, i.e. coupling a particle's canonical momentum with its (pseudo-) spin degrees of freedom [21, 22]. The realization of SOC provides an important ingredient for studying the fractional quantum Hall effect, topological insulators [23, 24], and has been a fundamental advancement in ultracold quantum gases in recent years [25, 26].

There are currently several experimental techniques to realize SOC in cold-atom systems, such as lattice shaking [27] and Raman coupling [28]. In particular, the Raman laser scheme has been applied to achieve one-dimensional SOC (an equal mixture of Rashba and Dresselhaus spin-orbit coupling) [28–33] and two-dimensional SOC [34–36] in ultracold gases of alkali atoms. However, Raman coupling for alkali atoms usually also comes along with atomic heating due to spontaneous emission. This heating leads to the loss of quantum degeneracy and trap population, which is a major challenge to study many-body quantum phenomena that manifest at a lower temperature and longer timescales. For atoms with higher ground state orbital angular momentum, spontaneous emission

can be eliminated while still producing large Raman coupling [37], making the open-shell lanthanide atoms Dy and Er suitable candidates. These elements also possess large magnetic dipole moment, allowing studies of the interplay between SOC and long-range dipole-dipole interactions that do not exist in alkali atomic gases, but requiring a more sophisticated theoretical model. Experimentally, SOC has been recently achieved by Ref. [38] in  $^{161}\text{Dy}$ , which allowed for the realization of a long-lived SOC degenerate dipolar Fermi gas. The bosonic system of SOC dipolar gas has also been theoretically investigated previously in BEC of  $^{52}\text{Cr}$  [39].

The existence of *long-range* dipole-dipole interactions in these systems is expected to give an interesting interplay with the SOC, leading to intriguing new quantum phases. Previous theoretical studies on the interplay between *short-range* two-body interactions and SOC in Fermi gases have explored novel superfluid states in the BEC-BCS crossover [40–44]. For a BEC with SOC, new quantum phases, such as a stripes phase, have been predicted for a certain range of the Raman coupling strengths determined by the inter- and intraspecies scattering lengths [45–48]. The anisotropic and long-range dipole-dipole interaction can be regarded as an additional degree of freedom, which might lead to new physics, but also brings new challenges in theoretical studies. To construct a concrete theoretical model for SOC dipolar quantum gases, the low-energy scattering between two dipoles in the presence of SOC needs to be understood first, which is the main topic of our study here.

Our theoretical formalism is inspired by several previous studies on ultracold collisions between two non-dipole particles in the presence of the three-dimensional (3D) isotropic SOC (which is a 3D analog of Rashba SOC) [49–54]. While the 3D isotropic SOC has not yet been realized experimentally in cold-atom systems, proposals have been made that are based on adding more laser fields. Recently, the realization of 2D isotropic SOC using this scheme has been reported [55]. The laser scheme to realize 3D isotropic SOC is ideally suited for lanthanide atoms, where there is less atomic heating. On the other hand, the 3D isotropic SOC is more closely related to the cases in condensed-matter physics due to the high

symmetry [56, 57]. This symmetry also allows for a fully analytical treatment of low-energy scattering in the presence of SOC.

The low-energy scattering is strongly affected by the asymptotic behavior of atoms at large distances. In our system, the SOC persists even for atoms with infinite separation, which changes the threshold energies, and modifies the dispersion relation [25]; on the other hand, a dipole-dipole interaction also dominates potential energies at large distances. The competition between SOC and dipole-dipole interaction, therefore, gives rise to special threshold behaviors. The details of our formalism to study this problem is outlined below in Sec. II. An analysis by applying the first-order Born approximation is given in Sec. III. A comparison with numerical results for spin-1/2 dipolar fermions is given in Sec. IV. A summary of our study is given in Sec. V.

## II. FORMALISM

In our model, each dipole is treated as a point particle with mass  $m$ . The interaction potential  $V(\vec{r})$  between two dipoles aligned to the  $z$ -axis and separated by a large distance  $\vec{r}$  is therefore given by  $V(\vec{r}) \rightarrow V_d(\vec{r}) = d^2(1 - 3\cos^2\theta)/r^3$ . Here  $\theta$  is the polar angle of  $\vec{r}$  in spherical coordinates, and  $d = \mu_m \sqrt{\mu_0/4\pi}$  denotes the dipole moment, where  $\mu_m$  is the magnetic dipole moment

and  $\mu_0$  is the vacuum permeability. The characteristic length scale of the dipole potential  $V_d(\vec{r})$  is given by the dipole length  $D = \mu d^2/\hbar^2$ , where  $\mu = m/2$  is the two-body reduced mass. Correspondingly, a natural energy scale can be defined by the dipole energy  $E_D = \hbar^2/\mu D^2$ . To mimic the experimentally available control of short-range interactions by using methods such as Feshbach resonances, we model the short-range potential by a simplistic hard-wall potential, i.e.  $V(\vec{r}) = V_d(\vec{r})$  for  $r \geq r_c$ , and  $V(\vec{r}) = \infty$  for  $r < r_c$ . This specific chosen form of the short-range potential, however, does not limit the generality of our study of ultracold collisions especially near potential resonances, which will be elaborated on later.

Similar to Refs. [49–54], we focus on the scattering in the center-of-mass frame. With the presence of 3D isotropic SOC, the Hamiltonian in relative coordinates is given by,

$$H = \frac{\vec{p}^2}{2\mu} + \frac{k_{\text{so}}}{2\mu} \vec{p} \cdot (\vec{s}_1 - \vec{s}_2) + V(\vec{r}), \quad (1)$$

where  $\vec{s}_1$  and  $\vec{s}_2$  are the spin operators for atom 1 and atom 2,  $\vec{p}$  is the relative momentum operator, and  $k_{\text{so}}$  is the strength of SOC in the units of inverse length. The energy scale for SOC can therefore be defined by the recoil energy  $E_r = \hbar^2 k_{\text{so}}^2/2m$ .

Following the same spirit as Refs. [51–54], we solve the relative Schrödinger equation formally as a multichannel problem, i.e. using channel functions (basis) of  $\Omega$ , all degrees of freedom except for  $r$ , to expand the  $\tau$ 'th independent solution as,

$$\Psi_\tau(\vec{r}) = \sum_\nu \Phi_\nu(\Omega) \frac{F_{\nu\tau}(r)}{r}. \quad (2)$$

The channel functions adopted here are the tensor spherical harmonics that are simultaneous eigenstates of  $\{\vec{j}^2, j_z, \vec{\ell}^2, \vec{s}^2\}$  whose eigenvalues are collectively represented by  $\nu$ . Here,  $\vec{\ell}$  is the (relative) orbital angular momentum operator,  $\vec{s} = \vec{s}_1 + \vec{s}_2$  is the total spin operator,  $\vec{j}$  is the total angular momentum, and  $j_z$  is the projection to the  $z$ -axis in the laboratory frame. The tensor spherical harmonics are defined as,

$$\Phi_\nu(\Omega) \equiv \langle \theta, \phi | (\ell s) j m_j \rangle = i^\ell \sum_{m_\ell, m_s} C_{\ell m_\ell; s m_s}^{j m_j} Y_{\ell m_\ell}(\theta, \phi) \chi(s, m_s), \quad (3)$$

where  $C_{\ell m_\ell; s m_s}^{j m_j}$  are the Clebsch-Gordan coefficients,  $Y_{\ell m_\ell}(\theta, \phi)$  are the usual spherical harmonics, and  $\chi(s, m_s)$  denote the spin states. The  $i^\ell$  phase term is introduced to make the matrix elements of the Hamiltonian all real, which will be convenient for carrying out numerical propagation later. The matrix elements for the first two terms in Eq. (1) (except for an additional phase associated with the  $i^\ell$  term) have been derived previously in Refs. [51, 52]:

$$\langle (\ell', s') j' m'_j | \frac{\vec{p}^2}{2\mu} | (\ell, s) j m_j \rangle \equiv \frac{\hbar^2}{2\mu} \left( -I_{\nu'\nu} \frac{d^2}{dr^2} + B_{\nu'\nu}^{(2)} \right) = \left( -\frac{\hbar^2}{2\mu} \frac{d^2}{dr^2} + \frac{\hbar^2 \ell(\ell+1)}{2\mu r^2} \right) \delta_{jj'} \delta_{m_j m'_j} \delta_{\ell\ell'} \delta_{ss'}, \quad (4)$$

and

$$\begin{aligned}
\langle (\ell', s') j' m'_j | \frac{k_{\text{so}}}{2\mu} \vec{p} \cdot (\vec{s}_1 - \vec{s}_2) | (\ell, s) j m_j \rangle &\equiv \frac{\hbar^2}{2\mu} \left( A_{\nu'\nu} \frac{d}{dr} + B_{\nu'\nu}^{(1)} \frac{1}{r} \right) \\
&= \delta_{jj'} \delta_{m_j m'_j} \left\{ \begin{matrix} s' & 1 & s \\ \ell & j & \ell' \end{matrix} \right\} (-1)^{j+\ell+s'+s_1+s_2} \\
&\times \left[ -(-1)^s \sqrt{s_1(s_1+1)(2s_1+1)} \left\{ \begin{matrix} s_1 & s_2 & s \\ s' & 1 & s_1 \end{matrix} \right\} + (-1)^{s'} \sqrt{s_2(s_2+1)(2s_2+1)} \left\{ \begin{matrix} s_2 & s_1 & s \\ s' & 1 & s'_2 \end{matrix} \right\} \right] \\
&\times \left( -\frac{\hbar^2 k_{\text{so}}}{2\mu} \right) \left[ \left( \frac{d}{dr} - \frac{\ell+1}{r} \right) \sqrt{\ell+1} \delta_{\ell', \ell+1} + \left( \frac{d}{dr} + \frac{\ell}{r} \right) \sqrt{\ell} \delta_{\ell', \ell-1} \right], \quad (5)
\end{aligned}$$

which are all real. Here, the curly bracket denotes the 6j symbol. Since the isotropic SOC preserves total angular momentum, different  $j$ 's are not coupled by these two terms. However, the anisotropic dipole-dipole interaction will couple different  $j$ 's, and only  $m_j$  is still a good quantum number due to the azimuthal symmetry. The matrix elements for dipole-dipole interaction are then given by,

$$\langle (\ell', s') j' m'_j | V_d(\vec{r}) | (\ell, s) j m_j \rangle \equiv \frac{\hbar^2}{2\mu} B_{\nu'\nu}^{(3)} \frac{1}{r^3} = -i^{\ell'-\ell} \frac{2d^2}{r^3} (-1)^{\ell'-\ell+s+j} \delta_{s's} \Pi_{\ell j \ell'} C_{j m_j; 20}^{j' m'_j} \left\{ \begin{matrix} \ell & s & j \\ j' & 2 & \ell' \end{matrix} \right\} \begin{pmatrix} \ell' & 2 & \ell \\ 0 & 0 & 0 \end{pmatrix}, \quad (6)$$

where  $\Pi_{\ell j \ell'} = \sqrt{2\ell+1} \sqrt{2j+1} \sqrt{2\ell'+1}$ . These matrix elements are also real despite the  $i^{\ell'-\ell}$  factor, since the 3-j symbol at the end of Eq. (6) ensure that  $\ell' - \ell = 0, \pm 2$ . In addition, the Clebsh-Gordan coefficient  $C_{j m_j; 20}^{j' m'_j}$  shows that  $m_j$  is a good quantum number and only channels with  $|j - j'| \leq 2$  can be coupled (specially, if  $m_j = 0$ , only channels with  $|j - j'| = 0, 2$  are coupled.) In principle, one needs to include channels with all possible angular momenta for an exact calculation, however, only a finite number of channels,  $j \leq j_{\text{max}}$ , are needed in practice to obtain a converged result for the scattering cross-sections, where  $j_{\text{max}}$  is sufficiently large (about 40 for our chosen parameters) [58].

In terms of these matrix elements, the Schrödinger equation in matrix form can then be written as,

$$\left( -\underline{I} \frac{d^2}{dr^2} + \underline{A} \frac{d}{dr} + \underline{B}(r) - k^2 \underline{I} \right) \underline{F}(r) = 0, \quad (7)$$

where the underlined variables,  $\underline{M}$ , denote matrices with matrix elements  $M_{\nu'\nu}$ ,  $\underline{I}$  is the identity matrix,  $E = \hbar^2 k^2 / 2\mu$  is the incident energy and  $\underline{B}(r) = \underline{B}^{(1)}/r + \underline{B}^{(2)}/r^2 + \underline{B}^{(3)}/r^3$ . The logarithmic derivative matrix  $\underline{\mathcal{L}} = \underline{F}' \underline{F}^{-1}$  can be obtained by propagating from  $r_c$  to a sufficiently large distance  $r_{\text{max}}$  (about  $10^4 D$  for our chosen parameters). The details of the propagation method is elaborated in Appendix A. The  $K$ -matrix and  $S$ -matrix are therefore given by,

$$\underline{\mathcal{K}} = (\underline{\mathcal{L}} \underline{g} - \underline{g}')^{-1} (\underline{\mathcal{L}} \underline{f} - \underline{f}'), \quad (8)$$

and

$$\underline{\mathcal{S}} = (\underline{I} + i\underline{\mathcal{K}})(\underline{I} - i\underline{\mathcal{K}})^{-1}, \quad (9)$$

respectively, where  $\underline{f}$  and  $\underline{g}$  are the regular and irregular solutions in matrix form.

The regular solutions  $\underline{f}$  are obtained by projecting the plane-wave solutions onto the tensor spherical harmonics, Eq. (3). The plane-wave solution with scattering energy

$E = \hbar^2 k^2 / 2\mu$  can be written as

$$\begin{aligned}
\langle \vec{r} | \xi, \zeta; +\hat{k} \rangle &= \sqrt{\frac{1}{2 + 2\delta_{\xi\zeta}}} \times \\
&\left[ e^{i\vec{k}_{\xi\zeta} \cdot \vec{r}} | \xi, +\hat{k} \rangle | \zeta, -\hat{k} \rangle + (-)^{p_b} e^{-i\vec{k}_{\xi\zeta} \cdot \vec{r}} | \zeta, -\hat{k} \rangle | \xi, \hat{k} \rangle \right], \quad (10)
\end{aligned}$$

where  $p_b$  equals 0 (1) for identical bosons (fermions) and  $| \xi, \hat{n} \rangle$  is a single-particle state with the projection of spin along the quantization axis  $\hat{n}$  being  $\hbar \xi$ . In the presence of 3D isotropic SOC, the particle can be well described by its helicity state, where the quantization axis is along the direction of its canonical momentum. Here  $\vec{k}_{\xi\zeta}$  is the canonical momenta with direction  $\vec{k}$  and magnitude  $k_{\xi\zeta} = \sqrt{k^2 + \kappa_{\xi\zeta}^2} - \kappa_{\xi\zeta}$ , where  $\kappa_{\xi\zeta} = (\xi + \zeta) k_{\text{so}} / 2$ . The expansion gives the matrix elements of  $\underline{f}$  as  $f_{\nu\tau} = u_{\nu\tau} k_{\tau} r j_l(k_{\tau} r) / \sqrt{N_{\tau}}$ , where  $N_{\tau} = \pi \hbar^2 \sqrt{k^2 + \kappa_{\xi\zeta}^2} / 2\mu$  is the normalization constant chosen to ensure flux density conservation, and

$$u_{\nu\tau} = \sqrt{\frac{2\ell+1}{2j+1}} C_{\ell, 0; s, \xi-\zeta}^{j, \xi-\zeta} C_{s_1, \xi; s_2, -\zeta}^{s, \xi-\zeta} \frac{1 + (-)^{s_1+s_2-s+\ell+p_b}}{\sqrt{2 + 2\delta_{\xi\zeta}}}. \quad (11)$$

Correspondingly, the matrix elements of the irregular solutions  $\underline{g}$  are given by  $g_{\nu\tau} = u_{\nu\tau} k_{\tau} r n_l(k_{\tau} r) / \sqrt{N_{\tau}}$ , where  $j_l$  and  $n_l$  are the regular and irregular spherical Bessel

functions respectively. Hereafter, unless specified otherwise, we use  $\nu = \{j, m_j, \ell, s\}$  to collectively represent the quantum numbers of the channel function in Eq. (3) and  $\tau = \{j, m_j, \xi, \zeta\}$  to represent the partial wave of a particular helicity state. Therefore, Eq. (11) can also be regarded as a unitary tranformation between the helicity basis denoted by  $\{\xi, \zeta\}$  and the spin singlet/triplet basis in the absence of SOC indicated by quantum number  $\{\ell, s\}$  for a particular partial wave of  $\{j, m_j\}$ . The explicit values of  $u_{\nu\tau}$  for spin-1/2 fermions and spin-1 bosons has been previously obtained for  $j = 0$  in Ref. [51] and Ref. [52] respectively, which can be used to verify our Eq. (11) (after carefully taking care of the  $i^\ell$  factor). The form of regular and irregular solutions guarantee the  $K$ -matrix to be real and symmetric (and hence the  $S$ -matrix to be unitary), where the proof is given in Appendix B.

Finally, the cross-section from one partial wave  $\{j', m'_j\}$  of helicity states  $\{\xi', \zeta'\}$  to another partial wave  $\{j, m_j\}$  of another helicity channel  $\{\xi, \zeta\}$  is given by,

$$\sigma_{\tau'\tau} = \frac{2\pi}{k_{\tau'}^2} |\mathcal{S}_{\tau'\tau} - \delta_{\tau'\tau}|^2. \quad (12)$$

### III. FIRST-ORDER BORN APPROXIMATION

One of the most important observables in ultracold collisions is the threshold law behavior determined by the competition between SOC, short-, and long-range interactions. In this work, we are mostly interested in magnetic dipolar atoms whose dipole lengths is about  $1 \sim 10$  nm for different species. Therefore, we are focusing on the case  $k_{\text{so}}D < 1$ , as the SOC strength is reasonably estimated to be  $k_{\text{so}} \approx 1 \sim 10 \mu\text{m}^{-1}$ . We remark that the parameter regime of  $k_{\text{so}}D > 1$  might be achieved in systems of heteronuclear molecules or Rydberg atoms, which is, however, beyond the scope of this paper.

The threshold behaviors for dipolar scattering without SOC have been discussed in Refs. [59–62], where the scattering cross-sections of partial waves with  $\ell > 0$  are universally determined by the dipole length. The physical explanation is that scattering at low energy can only occur at distances larger than the centrifugal barrier, where the potential is dominated by the dipole-dipole interaction. In addition, the  $1/r^3$  behavior of dipole-dipole interaction is weak at large distances, which allows the application of the perturbative first-order Born approximation. We apply the first-order Born approximation within the multi-channel framework, where the  $K$ -matrix can be approximated by [63, 64],

$$\mathcal{K}_{\tau'\tau}^{(\text{Born})} = \pi \int \sum_{\nu'\nu} f_{\nu'\tau'}^*(r) 2d^2 \frac{\tilde{B}_{\nu'\nu}^{(3)}}{r^3} f_{\nu\tau}(r) dr, \quad (13)$$

where  $\tilde{B}_{\nu'\nu}^{(3)} = B_{\nu'\nu}^{(3)}/4D$  by comparing with Eq. (6). Inserting the expression of the regular solution  $f_{\nu\tau}$ , we ar-

rive at,

$$\mathcal{K}_{\tau'\tau}^{(\text{Born})} = 4D \frac{\hbar^2 \pi}{2\mu} \frac{k_{\tau'} k_{\tau}}{\sqrt{N_{\tau'} N_{\tau}}} \sum_{\nu'\nu} u_{\nu'\tau'}^* \tilde{B}_{\nu'\nu}^{(3)} u_{\nu\tau} \Gamma_{\ell'\ell}^{\tau'\tau}, \quad (14)$$

where  $\Gamma_{\ell'\ell}^{\tau'\tau} = \int dr j_{\ell'}(k_{\tau'} r) j_{\ell}(k_{\tau} r) / r$ . Since we are in the perturbative regime, i.e.,  $\mathcal{K}_{\tau'\tau}^{(\text{Born})} \ll 1$ , the cross-section can be approximated by

$$\sigma_{\tau'\tau}^{(\text{Born})} \approx \frac{2\pi}{k_{\tau'}^2} |2\mathcal{K}_{\tau'\tau}^{(\text{Born})}|^2. \quad (15)$$

We would like to remark here that due to the absence of a centrifugal barrier in the  $s$ -wave channel, the first-order Born approximation should not apply to terms in the expansion when  $\ell' = \ell = 0$  as the integral  $\Gamma_{00}^{\tau'\tau}$  is divergent. However, this is not a problem, as  $\tilde{B}_{\nu'\nu}^{(3)} = 0$  for  $\ell' = \ell = 0$ , and hence gives no contribution to  $\mathcal{K}_{\tau'\tau}^{(\text{Born})}$ . Similar to the argument for the non-SOC case [59], the  $s$ -wave contributions can be included later by supplementing the Born approximation with a short-range contribution that can be determined from the full closed-coupling calculations.

The threshold behavior for partial waves satisfying the first-order Born approximations can be further explored by using the analytical properties of the integral  $\Gamma_{\ell'\ell}^{\tau'\tau}$ :

$$\Gamma_{\ell'\ell}^{\tau'\tau} = \left( \frac{k_{\tau'}}{k_{\tau}} \right)^{\ell'} \frac{\pi \Gamma[\frac{1}{2}(\ell + \ell')]}{8 \Gamma[\frac{1}{2}(3 + \ell - \ell')] \Gamma(\frac{3}{2} + \ell')} \times {}_2F_1\left[\frac{1}{2}(-1 - \ell + \ell'), \frac{1}{2}(\ell + \ell'), \frac{3}{2} + \ell', \frac{k_{\tau'}^2}{k_{\tau}^2}\right], \quad (16)$$

for  $k_{\tau} \geq k_{\tau'}$ , where  ${}_2F_1(a, b, c, z)$  is the hypergeometric function. Due to the symmetry of the integral, one can obtain  $\Gamma_{\ell'\ell}^{\tau'\tau}$  for  $k_{\tau} < k_{\tau'}$  by simply switching the primed and unprimed indices on the right-hand side. In addition, we only need to focus on the cases with  $\ell' - \ell = 0, \pm 2$ , since  $\tilde{B}_{\nu'\nu}^{(3)}$  equals zero otherwise. The integral can therefore be further simplified for  $k_{\tau} = k_{\tau'}$ ,

$$\Gamma_{\ell'\ell}^{\tau'\tau} = \begin{cases} \frac{1}{2\ell'(\ell'+1)}, & \ell' = \ell, \\ \frac{1}{6(\ell'+1)(\ell'+2)}, & \ell' = \ell - 2, \\ \frac{1}{6\ell'(\ell'-1)}, & \ell' = \ell + 2. \end{cases} \quad (17)$$

For  $k_{\tau} \neq k_{\tau'}$ , the integral can also be simplified in the limit  $k_{\tau'}/k_{\tau} \ll 1$ :

$$\Gamma_{\ell'\ell}^{\tau'\tau} \rightarrow \begin{cases} \frac{(\ell'-1)! 2^{\ell'-1}}{(2\ell'+1)!!} \left( \frac{k_{\tau'}}{k_{\tau}} \right)^{\ell'}, & \ell' = \ell, \\ \frac{\ell'! 2^{\ell'}}{3(2\ell'+1)!!} \left( \frac{k_{\tau'}}{k_{\tau}} \right)^{\ell'}, & \ell' = \ell - 2, \\ \frac{(\ell'-2)! 2^{\ell'-2}}{(2\ell'+1)!!} \left( \frac{k_{\tau'}}{k_{\tau}} \right)^{\ell'}, & \ell' = \ell + 2. \end{cases} \quad (18)$$

where the (double) exclamation marks denote a (double) factorial.

We remark here that, at the regime  $k_{\text{so}}D \ll kD \ll 1$ ,  $k_{\tau} \approx k_{\tau'} \approx k$ ,  $\Gamma_{\ell'\ell}^{\tau'\tau}$  can therefore always be approximated

by Eq. (17). Furthermore, if we investigate the case of  $s_1 = s_2 = 0$  (and therefore  $j = \ell$ ,  $j' = \ell'$  and  $m_j = m_{j'} = m_\ell$ ), one can verify that  $|2\mathcal{K}_{\tau'\tau}^{(\text{Born})}| \approx |\delta_{\tau'\tau} - \mathcal{S}_{\tau'\tau}^{(\text{Born})}|$  agrees with the  $T$ -matrix element  $|T_{\ell'\ell}^{(m_\ell), \text{Born}}|$  found in Ref. [59, 61] for dipole-dipole scattering without the presence of SOC.

#### IV. EXAMPLE: TWO SPIN-1/2 FERMIONIC DIPOLES

We apply our analysis to systems of two identical spin-1/2 fermionic dipoles as an example, and focus on the  $m_j = 0$  and even  $j$  channels. In order to simplify notation we use  $+$  and  $-$  to represent the helicity  $+1/2$  and  $-1/2$  respectively in this section. Furthermore, to avoid double counting, we always choose  $\xi < \zeta$ . Therefore, the three possible two-particle helicity states for the two dipoles are given by  $(\xi, \zeta) = (-, -)$ ,  $(-, +)$  and  $(+, +)$ , with canonical momentum  $k_{--} = \sqrt{k^2 + (k_{\text{so}}/2)^2} + k_{\text{so}}/2$ ,  $k_{-+} = k$ , and  $k_{++} = \sqrt{k^2 + (k_{\text{so}}/2)^2} - k_{\text{so}}/2$ , and normalization constant  $N_{--} = N_{++} = \pi\hbar^2\sqrt{k^2 + (k_{\text{so}}/2)^2}/2\mu$ , and  $N_{-+} = \pi\hbar^2\sqrt{k}/2\mu$ . Using Eq. (11), we find that for  $j = 0$ , only  $(-, -)$  and  $(+, +)$  are involved and coupled to the channel functions  $\nu = \{j = 0, m_j = 0, \ell = 0, s = 0\}$  and  $\{0, 0, 1, 1\}$ . For higher even  $j$ 's, all three possible helicity states are involved and coupled to  $\nu = \{j, 0, j, 0\}$ ,  $\{j, 0, j - 1, 1\}$  and  $\{j, 0, j + 1, 1\}$ . Therefore, only the partial waves with  $j = 0$  are coupled to  $s$ -wave, and the first-order Born approximation can be applied to all other higher partial waves.

Some of the elastic scattering cross-sections and corresponding  $K$ -matrix elements are shown in Fig. 1. The solid curves are numerical calculations using parameters  $k_{\text{so}}D = 0.1$  and  $r_c = 0.22D$ , while the dashed curves are the first-order Born approximations found from Eq. (14) and Eq. (15). The first-order Born approximation agrees excellently with the essentially exact calculations at low scattering energy (small  $k$ ) and high angular momentum partial waves. The almost perfect agreement can be understood by realizing the scattering occurs at larger distances for lower scattering energy and a higher centrifugal barrier, where the first-order Born approximation becomes almost exact.

The first-order Born approximation also agrees well for the essentially numerically exact inelastic process. In Fig. 2, we present some inelastic cross-sections and the corresponding  $K$ -matrix elements from channels of  $(j, m_j) = (2, 0)$  to  $(4, 0)$ , but the state remains in the same helicity, which also show very good agreement. We can write out the explicit form for the elastic and inelastic cross-sections whose incoming and outgoing two-particle

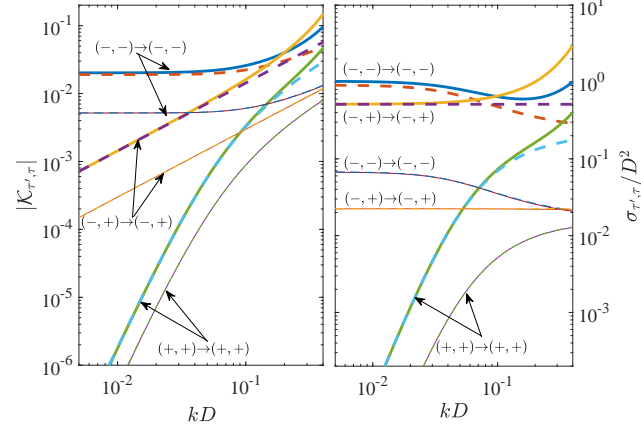


Figure 1. (Color online)  $K$ -matrix elements and cross-sections for elastic scattering in channels of  $(j, m_j) = (2, 0)$ , represented by the thick curves and  $(4, 0)$ , by the thin curves. The incoming and outgoing helicity states for each curve are indicated on the figure. The solid curves are results from numerical calculation with  $k_{\text{so}}D = 0.1$  and  $r_c = 0.22D$ , compared with the dashed curves from the first-order Born approximation. For the  $(j, m_j) = (4, 0)$  channels, the dashed curves and solid curves are essentially on top of each other and cannot be distinguished visually at this scale.

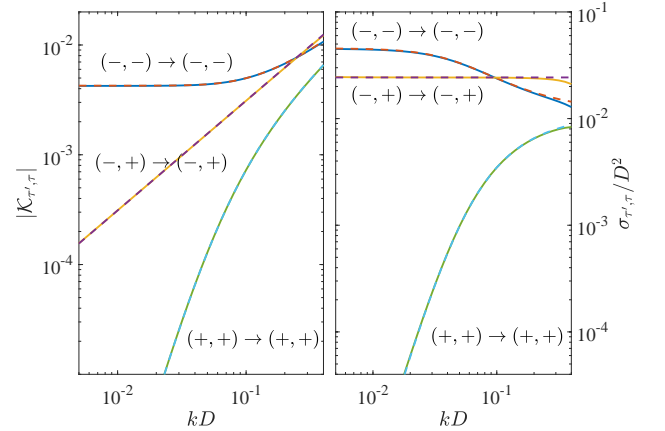


Figure 2. (Color online)  $K$ -matrix elements and cross-sections for inelastic scattering from channels of  $(j, m_j) = (2, 0)$  to  $(4, 0)$ , where the scattered state remains the same helicity. Other parameters and notation are the same as Fig. 1.

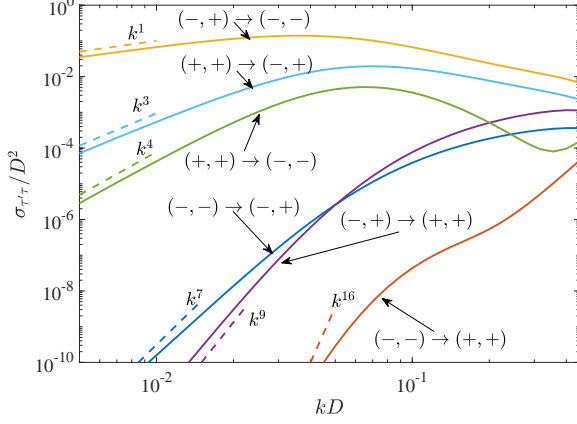


Figure 3. (Color online) The cross-sections for inelastic scattering that changes helicity from channels of  $(j, m_j) = (2, 0)$  to  $(4, 0)$ , where the initial and final helicity are indicated on the figure. The solid curves are numerical calculations with the same parameters as Fig. 1. The dashed curves show the corresponding power law.

helicity states are the same:

$$\sigma_{(-)\rightarrow(-)}^{j,m_j \rightarrow j',m'_j} = 128\pi D^2 C_{\tau'\tau}^2 \frac{\left(\sqrt{k^2 + (k_{\text{so}}/2)^2} + k_{\text{so}}/2\right)^2}{k^2 + (k_{\text{so}}/2)^2}, \quad (19)$$

$$\sigma_{(-+)\rightarrow(-+)}^{j,m_j \rightarrow j',m'_j} = 128\pi D^2 C_{\tau'\tau}^2, \quad (20)$$

$$\sigma_{(++)\rightarrow(++)}^{j,m_j \rightarrow j',m'_j} = 128\pi D^2 C_{\tau'\tau}^2 \frac{\left(\sqrt{k^2 + (k_{\text{so}}/2)^2} - k_{\text{so}}/2\right)^2}{k^2 + (k_{\text{so}}/2)^2}, \quad (21)$$

where  $C_{\tau'\tau} = \sum_{\nu'\nu} u_{\nu'\tau'}^* \tilde{B}_{\nu'\nu}^{(3)} u_{\nu\tau} \Gamma_{\ell'\ell}^{\tau'\tau}$  is a constant with respect to  $k$ , and  $\Gamma_{\ell'\ell}^{\tau'\tau}$  is given by Eq. (17). The threshold power law at  $k \ll k_{\text{so}}$  can therefore be given by  $\sigma_{(-)\rightarrow(-)}^{j,m_j \rightarrow j',m'_j} \rightarrow k^0$ ,  $\sigma_{(-+)\rightarrow(-+)}^{j,m_j \rightarrow j',m'_j} \rightarrow k^0$ , and  $\sigma_{(++)\rightarrow(++)}^{j,m_j \rightarrow j',m'_j} \rightarrow k^4$ .

For inelastic scattering processes with different incoming and outgoing helicity states, simple formulas for cross-sections without involving the hypergeometric function do not exist. However, in the limit  $k \ll k_{\text{so}}$ , the threshold behavior can still be analyzed by using Eq. (18). For example, in the process  $\tau' = \{2, 0, -, +\} \rightarrow \tau = \{4, 0, -, -\}$ , we have  $k_{-+}/k_{--} \rightarrow k$  in the low  $k$  limit, which leads to  $\Gamma_{\ell'\ell}^{\tau'\tau} \rightarrow k^{\ell'}$ . Therefore, the leading order of the  $K$ -matrix element is  $\mathcal{K}_{\tau'\tau} \rightarrow k^{\ell_{\text{min}}+1/2}$ , where  $\ell_{\text{min}}$  is the lowest  $\ell'$  that can couple to  $j' = 2$ , which equals 1 in this case. The additional factor of  $1/2$  in the exponent comes from the factor  $k_{\tau'} k_{\tau} / \sqrt{N_{\tau'} N_{\tau}}$ . The cross-section, therefore, obeys the power law  $\sigma_{\tau'\tau} \rightarrow k^1$ . The same analysis can be applied to other scattering processes, and are summarized in Fig. 3 for cross-sections from channels of  $(j, m_j) = (2, 0)$  to  $(4, 0)$ . We can see that the

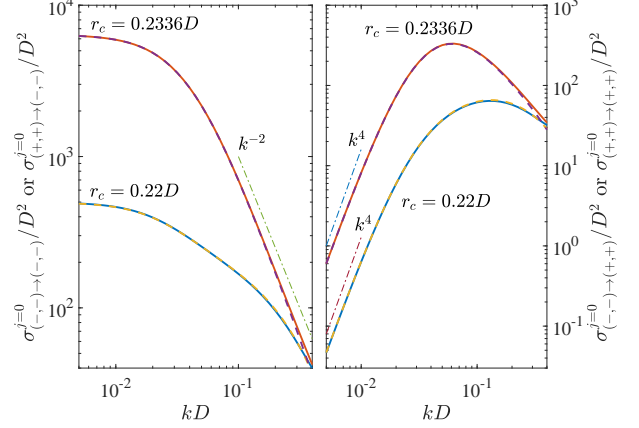


Figure 4. (Color online) The cross-sections in the subspace of  $(j, m_j) = (0, 0)$ . In the left panel, the solid/dashed curves shows the cross-sections from  $(-, -)/(+, +)$  to  $(-, -)$  helicity states, and in the right panel, the solid/dashed curves shows the cross-sections from  $(+, +)/(-, -)$  to  $(+, +)$  respectively. These are numerical calculation results with  $k_{\text{so}}D = 0.05$  and different  $r_c$  indicated on the figure. For the same set of parameters, the solid and dashed curves are essentially on top of each other in this scale.

power-law describes the threshold behaviors well.

We have also carried out calculations for different  $r_c$ , and observe that the cross-sections for  $j > 0$  discussed previously are insensitive to  $r_c$ , i.e., the cross-sections at low scattering energy are universally determined by the dipole length  $D$  and  $k_{\text{so}}$ . This universality also applies better for lower  $k$  and higher angular momentum  $j$  due to the better application of the first-order Born approximation. However, for the partial cross-sections in the subspace of  $j = 0$ , the universality implied by the first-order Born approximation no longer exist due to the absence of a centrifugal barrier. Indeed, we find that the cross-section in the subspace of  $j = 0$  depends on  $r_c$  and can change by orders of magnitude in our numerical calculation, as shown in Fig. 4. One can also see that the cross-sections in the  $j = 0$  subspace share a lot of similarities with the short-range results presented in Ref. [51], such as the power-law behaviors, and the identical cross-sections for the same final helicity state regardless of the initial helicity state at very small  $k$ .

In addition, the cross-sections for final states  $(-, -)$  at low scattering energy goes to a constant and can reach resonance by tuning  $r_c$ , similar to the non-SOC situation studied in Ref. [65]. In particular, near the broad potential resonances found in Ref. [65] (or more specifically, away from shape resonances and closed-channel dominated resonances), we have observed another universality, i.e., the cross-section can be universally determined by the dipole length  $D$ , SOC coupling  $k_{\text{so}}$ , and the non-SOC singlet  $s$ -wave scattering length  $a_s$ . This universality implies that all the short-range physics can be absorbed into one single parameter  $a_s$ , and the detailed form of

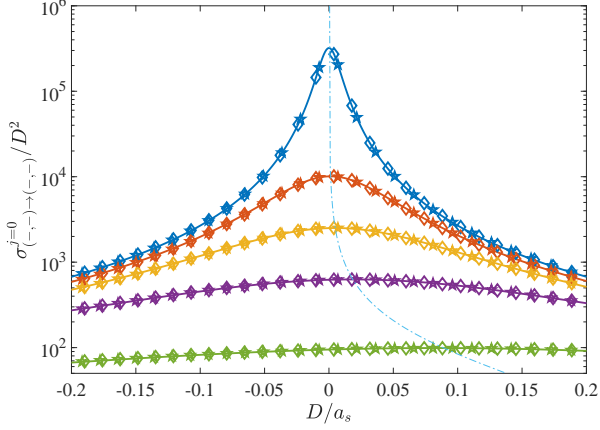


Figure 5. (Color online) Elastic cross-sections for the helicity state  $(-, -)$  in the subspace of  $(j, m_j) = (0, 0)$  for different  $k_{so}$  as a function of non-SOC singlet  $s$ -wave scattering length  $a_s$ . The curves from top to bottom are corresponding to  $k_{so}D = 0.01, 0.05, 0.1, 0.2$ , and  $0.5$ . The diamond (pentagram) symbols are numerical results calculated near the resonance at  $r_c \approx 0.232D$  ( $0.103D$ ). The solid curves are fitted using Eq. (22). The dash-dotted curve guides the position of resonances.

the short-range interaction is not important. The underlying physics is the classical suppression of the WKB wave function amplitude by the large potential well at short distances [11], where a frame transformation is allowed. Therefore, we do not expect this universality can be applied to shape-resonances or closed-channel dominated resonances, where details of short-range potential becomes important.

As shown in Fig. 5, for a fixed  $k_{so}D$ , the elastic cross-sections  $\sigma_{(-,-) \rightarrow (-,-)}^{j=0}$  are calculated near two different resonances and can be fitted as a function of  $a_s/D$ ,

$$\sigma_{(-,-) \rightarrow (-,-)}^{j=0}/D^2 = \frac{\sigma_{\text{res}}/D^2}{(D/a_s - D/a_{\text{res}})^2/\Gamma_{\text{res}}^2 + 1}, \quad (22)$$

where  $\sigma_{\text{res}}$ ,  $a_{\text{res}}$ , and  $\Gamma_{\text{res}}$  are fitting parameters, which only depend on  $k_{so}D$ . Figure 5 also shows the effect of  $k_{so}$  on resonances: the resonance shifts further to the positive side and becomes broader for larger SOC coupling. Interestingly, the shift of resonance due to the presence of SOC can be explained by the interplay between the short-range interaction and SOC (see Appendix C for details).

Another interesting feature in ultracold scattering with the presence of SOC is that the particles are preferentially scattered into the lowest helicity states (where the particle's momentum is antiparallel to its spin direction), regardless of their incidence channel [51, 60]. This spontaneous handedness is an analog of an antiferromagnetic phenomena induced by the momentum-dependent magnetic field. The presence of dipole-dipole interaction would not change this spontaneous handedness effect, as

can be seen by comparing the ratios of the different scattering cross-sections  $\sigma_{\tau'\tau}/\sigma_{\tau\tau'} = k_{\tau'}^2/k_{\tau}^2$ . Therefore, after sometime, we expect all the particles in our system to be in a “ $-$ ” helicity state, and any rethermalization due to a perturbation should be described by the total cross-section of  $\sigma_{(-,-) \rightarrow (-,-)}^{\text{tot}} = \sigma_{(-,-) \rightarrow (-,-)}^{j=0} + \sigma_{(-,-) \rightarrow (-,-)}^{(\text{Born})}$ , where

$$\sigma_{(-,-) \rightarrow (-,-)}^{(\text{Born})} = \sum_{j,j',m_j} \sigma_{(-,-) \rightarrow (-,-)}^{j,m_j \rightarrow j',m_j}. \quad (23)$$

Summing the partial cross-section from Eq. (19) in the limit of  $k \rightarrow 0$  gives  $\sigma_{(-,-) \rightarrow (-,-)}^{\text{tot}} \approx \sigma_{(-,-) \rightarrow (-,-)}^{j=0} + 4.46D^2$ . Noticing that  $(32\pi D^2/15 + 32\pi D^2/45)/2 \approx 4.46D^2$  implies that the total cross-section from the first-order Born approximation equals the average of cross-sections for identical fermions ( $32\pi D^2/15 \approx 6.70D^2$ ) and identical bosons ( $32\pi D^2/45 \approx 2.23D^2$ ) without the presence of SOC [61, 66]. We believe this reflects the fact that the total cross-section sums over the singlet and triplet cross-sections, which corresponds to the non-spin identical bosons and fermions respectively. In addition, when the particles are in  $(-, -)$  helicity, they have equal probability to be projected into singlet and triplet states.

## V. CONCLUSION

In summary, this paper extends previous theoretical studies of ultracold scattering in the presence of 3D isotropic SOC to a dipolar system. Our formalism is general in the sense that it can be applied to either bosons or fermions with arbitrary spin and the inclusion of any angular momentum partial waves. Similar to the non-SOC cases, the cross-sections involving high angular momentum partial waves can be well described by the first-order Born approximation, and can be determined universally by the dipole length  $D$  and spin-orbit coupling strength  $k_{so}$ . However, the cross-sections that can couple to an  $s$ -wave channel depend on the short-range physics and can have resonances. Nevertheless, all the short-range physics can be described by one additional parameter,  $a_s$ , near a broad potential resonance. We have tested our theory in the example system of spin-1/2 dipolar fermions, and find excellent agreement with our numerical calculations.

While this work focuses on the ultracold regime  $E \rightarrow 0^+$ , our formalism can be easily extended to the negative scattering energy  $E = -\kappa^2/2\mu$  following the same approach in Ref. [53]. In this energy regime, however, the canonical momentum should be understood as given by  $k_{\xi\xi} = \sqrt{\kappa_{\xi\xi}^2 - \kappa^2} - \kappa_{\xi\xi}$  (which has the same definition of  $\bar{k}$  in Ref. [53]). This topic, however, will be addressed elsewhere in the future.



## ACKNOWLEDGMENTS

We would like to thank Hui Hu for his insightful discussions. This research was supported under Australian Research Council's Future Fellowships funding scheme (project number FT140100003) and Discovery Projects funding scheme (project number DP170104008). The numerical calculations were partly performed using Swinburne new high-performance computing resources (Green II).

## Appendix A: Propagation Method

Based on the R-matrix propagation method using discrete variable representations (DVR) basis, we develop a numerically stable method for propagating the logarithmic derivative matrix  $\underline{\mathcal{L}} = \underline{F}' \underline{F}^{-1}$ , where  $\underline{F}$  is the solution of Eq. (7). Numerically, we separate the whole regime into many sectors. For each sector  $r \in [a_1, a_2]$  the propagation method allows us to calculate the logarithmic derivative matrix at one end  $\underline{\mathcal{L}}(a_2)$  for a given  $\underline{\mathcal{L}}(a_1)$  on the other end. One key ingredient in this method is the construction of the DVR basis. Our DVR basis functions  $\pi_j(r)$  are in the form of Langrange polynomial:

$$\pi_i(r) = \sqrt{\frac{1}{\tilde{w}_i}} \prod_{j \neq i}^N \frac{r - r_j}{r_i - r_j}, \quad (\text{A1})$$

where  $r_i = sx_i + \bar{a}$  and  $\tilde{w}_i = sw_i$  are defined by the  $N$  Gauss-Lobatto quadrature points  $x_i$  and weights  $w_i$  correspondingly, with  $s = (a_2 - a_1)/2$  and  $\bar{a} = (a_2 + a_1)/2$  [67]. One can easily verify that a DVR basis satisfies  $\pi_i(r_j) = \delta_{ij}/\sqrt{\tilde{w}_i}$  that leads to the DVR approximation, i.e.  $\int_{a_1}^{a_2} \pi_i(r) v(r) \pi_j(r) dr \approx v(r_i) \delta_{ij}$  with a smooth function  $v(r)$ . In addition, the derivative of DVR basis  $\pi'_i(r)$  can be derived analytically.

Under the DVR approximation, Eq. (7) can be written as,

$$\underline{H} \underline{\vec{c}}^{(\mu)} \equiv (\underline{T} + \underline{M} + \underline{V} - k^2 \underline{I}) \underline{\vec{c}}^{(\mu)} = \underline{A} \underline{\vec{c}}^{(\mu)}, \quad (\text{A2})$$

after integrating by parts, where  $c_{\nu j}^{(\mu)}$  (in vector notation,  $\vec{c}^{(\mu)}$ ) are the expansion coefficients for the matrix elements of  $\underline{F}$ ,

$$F_{\nu\mu}(r) = \sum_j c_{\nu j}^{(\mu)} \pi_j(r). \quad (\text{A3})$$

The matrix elements of other terms in Eq. (A2) are given by

$$T_{\mu i, \nu j} = \delta_{\mu\nu} \sum_m \tilde{w}_m \pi'_i(r_m) \pi'_j(r_m), \quad (\text{A4})$$

$$M_{\mu i, \nu j} = A_{\mu\nu} \frac{1}{2} \sum_m \tilde{w}_m [\pi_i(r_m) \pi'_j(r_m) - \pi'_i(r_m) \pi_j(r_m)], \quad (\text{A5})$$

$$V_{\mu i, \nu j} = B_{\mu\nu}(r_i) \delta_{ij}, \quad (\text{A6})$$

which are all symmetric. The surface term is given by

$$\Lambda_{\mu i, \nu j} = \{\pi_i(r) [\delta_{\mu\nu} \pi'_j(r) - \frac{1}{2} A_{\mu\nu} \pi_j(r)]\}_{a_1}^{a_2}. \quad (\text{A7})$$

From the form of the surface term, we define a matrix  $\underline{L} = \underline{\mathcal{L}} - \underline{A}/2$ , so that we have,

$$\underline{F}'(r) = \left[ \underline{L}(r) + \frac{1}{2} \underline{A} \right] \underline{F}(r), \quad (\text{A8})$$

which gives,

$$\sum_{j\nu} \Lambda_{i\tau, j\nu} c_{j\nu}^{(\mu)} = \sum_{\nu} \left[ \frac{\delta_{iN} \delta_{jN}}{\tilde{w}_N} L_{\mu\nu}(a_2) c_{\nu N}^{(\mu)} - \frac{\delta_{i1} \delta_{j1}}{\tilde{w}_1} L_{\mu\nu}(a_1) c_{\nu 1}^{(\mu)} \right]. \quad (\text{A9})$$

Defining the matrix  $\underline{h}^{cc'}$  with the elements

$$h_{i\tau, j\nu}^{cc'} = \underline{H}_{i\tau, j\nu} + \frac{\delta_{i1} \delta_{j1}}{\tilde{w}_1} L_{\mu\nu}(a_1), \quad (\text{A10})$$

where  $c$  and  $c'$  are a collective index for selected DVR basis indices, i.e.  $i \in c$  and  $j \in c'$ . The radial equation can therefore be written in a matrix form:

$$\begin{pmatrix} h^{ss} & h^{sN} \\ h^{Ns} & h^{NN} \end{pmatrix} \begin{pmatrix} \vec{c}_s^{(\mu)} \\ \vec{c}_N^{(\mu)} \end{pmatrix} = \begin{pmatrix} 0 & 0 \\ 0 & L(a_2)/\tilde{w}_N \end{pmatrix} \begin{pmatrix} \vec{c}_s^{(\mu)} \\ \vec{c}_N^{(\mu)} \end{pmatrix}, \quad (\text{A11})$$

which leads to

$$\frac{1}{\tilde{w}_N} \underline{L}(a_2) = \underline{h}^{NN} - \underline{h}^{Ns} \frac{1}{\underline{h}^{ss}} \underline{h}^{sN}, \quad (\text{A12})$$

with  $s = 1, 2, \dots, N-1$ . For the first sector, if we impose a hard-wall boundary condition from the left, i.e.  $F(a_1) = 0$ , a special treatment has to be implemented for this sector. Notice that only the first DVR basis  $\pi_1(r)$  has non-zero value at  $a_1$ , the boundary condition can be easily satisfied by choosing  $s = 2, \dots, N-1$  for the first sector. An additional feature from this formalism is that one can easily see that  $\underline{L}(a_2)$  is automatically real and symmetric if  $\underline{L}(a_1)$  is real and symmetric, implying  $\underline{L}$  is real and symmetric everywhere if we impose the hard-wall boundary condition.

## Appendix B: Symmetry of $K$ -matrix

As we will show later, the  $K$ -matrix  $\underline{K}$  is real and symmetric (correspondingly, the  $S$ -matrix  $\underline{S}$  is a unitary matrix) as long as  $\underline{L}$  is real and symmetric. We have already



shown that  $\underline{L}$  is real and symmetric in the DVR formulation. Below, we give a more general proof without the help of any specific radial basis. From the definition of  $\underline{L}$ , we have,

$$F' - \frac{1}{2}AF = LF. \quad (\text{B1})$$

From hereon in this section, we neglect the underline for matrix variables to symplify the notation. From the radial equation Eq. (7), we have,

$$F'' = AF + B - k^2I. \quad (\text{B2})$$

After some algebra, the derivative of  $L$  is given by,

$$L' = B - k^2I + \left(\frac{1}{2}A - L\right)F'F^{-1}. \quad (\text{B3})$$

The definition of  $L$  can also be re-written as

$$F'F^{-1} = \frac{1}{2}A + L. \quad (\text{B4})$$

Finally, we have,

$$L' = B - k^2I + \left(\frac{1}{2}A - L\right)\left(\frac{1}{2}A + L\right). \quad (\text{B5})$$

Notice that  $B$  is real and symmetric, and  $A$  is real and antisymmetric. Therefore, if  $L$  is real and symmetric,  $L'$  must also be real and symmetric, which implies  $L$  is real and symmetric at all points as long as it is real and symmetric at one point, which is usually satisfied at the origin.

In order to show that  $\underline{K}$  is also real and symmetric, we need to apply the properties of Wronskian of the regular and irregular solutions given by [52],

$$f'^T f - f^T f' + f^T A f = 0, \quad (\text{B6})$$

$$g'^T g - g^T g' + g^T A g = 0, \quad (\text{B7})$$

and

$$f'^T g - f^T g' + f^T A g = \frac{1}{\pi}I. \quad (\text{B8})$$

The radial wave function can be expressed in terms of these regular and irregular solutions as  $F = f - gK$ . Since  $f$  and  $g$  are both real,  $K$  is automatically guaranteed to be real. Substituting the regular and irregular solution into the definition of  $L$  gives,

$$(f' - g'K) - \frac{1}{2}A(f - gK) = L(f - gK), \quad (\text{B9})$$

which can be rewritten as,

$$L^{-1} \left[ (f' - g'K) - \frac{1}{2}A(f - gK) \right] = (f - gK), \quad (\text{B10})$$

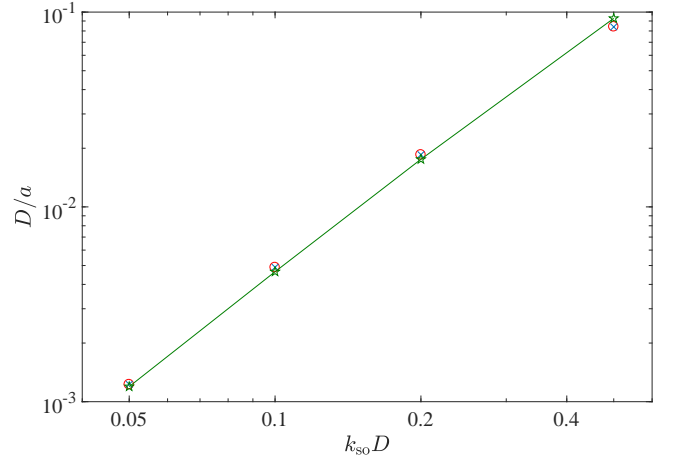


Figure 6. (Color online) Comparison of  $D/a_s^*$  (shown by green pentagrams) and  $D/a_{res}$  [shown by red circles (blue crosses) for resonance near  $r_c \approx 0.232D$  ( $r_c \approx 0.103D$ )] as a function of SOC strength  $k_{so}D$ .

and

$$(f^T - K^T g^T)L = (f'^T - K^T g'^T) + \frac{1}{2}(f^T - K^T g^T)A. \quad (\text{B11})$$

Multiplying both the left and right-hand-side of these two equations gives,

$$(f^T - K^T g^T) \left[ (f' - g'K) - \frac{1}{2}A(f - gK) \right] = \left[ (f'^T - K^T g'^T) + \frac{1}{2}(f^T - K^T g^T)A \right] (f - gK). \quad (\text{B12})$$

With the help of Wronskian, the above equation gives  $K = K^T$ , proving that  $K$  is symmetric.

Since  $K$  is real and symmetric, there exists a unitary transformation  $U$  that can diagonalize  $K$ :  $U^\dagger K U = \kappa$ , where  $\kappa$  is a diagonalized and real matrix. This unitary transformation  $U$  can also diagonalize  $I + iK$  and  $I - iK$ , which implies,

$$S \equiv (I + iK)(I - iK)^{-1} = (I - iK)^{-1}(I + iK), \quad (\text{B13})$$

is a unitary matrix.

### Appendix C: Frame Transformation

One elegant discovery in Ref. [54] is that, a frame transformation can be found if the atom-atom interaction is short-range. Here, we extend their approach from the distinguishable particle case to the identical particle case. Under such a transformation, the short-range hamiltonian  $H^{SR}$  and the free-space hamiltonian  $H^{FS}$  are analytically related by,

$$H^{SR} = H^{FS} + \frac{E_r}{2\hbar^2}[(\vec{s}_1 - \vec{s}_2) \cdot \vec{r}, (\vec{s}_1 - \vec{s}_2) \cdot \vec{\nabla}], \quad (\text{C1})$$

where  $E_r = \hbar k_{so}^2/2m$ . Noticing that our definition of  $k_{so}$  has a factor of two different than the one defined in Ref. [54]. For spin-1/2 atoms,  $\vec{s}_n = \hbar\vec{\sigma}^{(n)}/2$ , where  $\vec{\sigma}^{(n)}$  is a vector whose components are the three Pauli matrices for the particle  $n$ . For identical particles, the second term of the right-hand-side of Eq. (C1) can be simplified as,

$$\varepsilon = -\frac{E_r}{2\hbar^2} \left[ \vec{l} \cdot \vec{s} + (\vec{s}_1 - \vec{s}_2)^2 \right], \quad (C2)$$

where  $\vec{s} = \vec{s}_1 + \vec{s}_2$  is the total spin operator. Using tensor spherical harmonics to expand this operator gives a diagonal matrix for two spin-1/2 particles

$$\varepsilon_\nu = -\frac{E_r}{4} [j(j+1) - \ell(\ell+1) - s(s+1) + 6], \quad (C3)$$

where  $\nu = \{j, m_j, \ell, s\}$  are the quantum numbers for the tensor spherical harmonics. In the spirit of frame transformation [54], this effectively replaces the short-range parameter (scattering phase shift)  $\delta_\nu(k)$  by  $\delta_\nu(k_\nu)$ , where

$\hbar^2 k_\nu^2/2\mu = E - \varepsilon_\nu = \hbar^2 k^2/2\mu - \varepsilon_\nu$ . Near a  $s$ -wave resonance in free-space, the  $K$ -matrix reaches resonance if  $1/a_s(k_s) \rightarrow 0$ , where  $\hbar^2 k_s^2/2\mu = \hbar^2 k^2/2\mu + 3E_r/2$ .

In the presence of long-range and anisotropic dipole-dipole interaction, a direct application of the approach in Ref. [54] is not appropriate. However, we find that the resonance shift near an  $s$ -wave resonance described in Fig. 5 can still be understood via this approach, since the interplay between the short-range interaction and SOC plays an important role here. Near the resonance of  $r_c \approx 0.232D$  without the presence of SOC, we calculate the value of  $s$ -wave scattering length  $a_s^* = a_s(0)$  if the corresponding potential parameters gives  $1/a_s(k_s) \rightarrow 0$ . Interestingly, as illustrated in Fig. 6, the values of  $a_s^*$  agrees well with  $a_{res}$  in Eq. (22) that is calculated by fitting the resonance of a numerical calculation with the presence of SOC, clearly showing the shift of the resonance position is a result of interplay between a short-range interaction and SOC.

- 
- [1] F. Dalfovo, S. Giorgini, L. P. Pitaevskii, and S. Stringari, Rev. Mod. Phys. **71**, 463 (1999).
  - [2] A. J. Leggett, Rev. Mod. Phys. **73**, 307 (2001).
  - [3] I. Bloch, J. Dalibard, and W. Zwerger, Rev. Mod. Phys. **80**, 885 (2008).
  - [4] S. Giorgini, L. P. Pitaevskii, and S. Stringari, Rev. Mod. Phys. **80**, 1215 (2008).
  - [5] C. Chin, R. Grimm, P. Julienne, and E. Tiesinga, Rev. Mod. Phys. **82**, 1225 (2010).
  - [6] K. M. O'Hara, S. L. Hemmer, M. E. Gehm, S. R. Granade, and J. E. Thomas, Science **298**, 2179 (2002).
  - [7] P. Makotyn, C. E. Klauss, D. L. Goldberger, E. A. Cornell, and D. S. Jin, Nat. Phys. **10**, 116 (2014).
  - [8] M.-G. Hu, M. J. Van de Graaff, D. Kedar, J. P. Corson, E. A. Cornell, and D. S. Jin, Phys. Rev. Lett. **117**, 055301 (2016).
  - [9] T. Kraemer, M. Mark, P. Waldburger, J. G. Danzl, C. Chin, B. Engeser, A. D. Lange, K. Pilch, A. Jaakkola, H.-C. Nägerl, and R. Grimm, Nature **440**, 315 (2006).
  - [10] M. Berninger, A. Zenesini, B. Huang, W. Harm, H.-C. Nägerl, F. Ferlaino, R. Grimm, P. S. Julienne, and J. M. Hutson, Phys. Rev. Lett. **107**, 120401 (2011).
  - [11] J. Wang, J. P. D'Incao, B. D. Esry, and C. H. Greene, Phys. Rev. Lett. **108**, 263001 (2012).
  - [12] L. Santos, G. V. Shlyapnikov, and M. Lewenstein, Phys. Rev. Lett. **90**, 250403 (2003).
  - [13] L. Santos, G. V. Shlyapnikov, P. Zoller, and M. Lewenstein, Phys. Rev. Lett. **85**, 1791 (2000).
  - [14] A. Griesmaier, J. Werner, S. Hensler, J. Stuhler, and T. Pfau, Phys. Rev. Lett. **94**, 160401 (2005).
  - [15] T. Koch, T. Lahaye, J. Metz, B. Fröhlich, A. Griesmaier, and T. Pfau, Nat. Phys. **4**, 218 (2008).
  - [16] K.-K. Ni, S. Ospelkaus, M. H. G. de Miranda, A. Pe'er, B. Neyenhuis, J. J. Zirbel, S. Kotochigova, P. S. Julienne, D. S. Jin, and J. Ye., Science **322**, 231 (2008).
  - [17] T. M. Rvachov, H. Son, A. T. Sommer, S. Ebadi, J. J. Park, M. W. Zwierlein, W. Ketterle, and A. O. Jamison, Phys. Rev. Lett. **119**, 143001 (2017).
  - [18] M. Lu, S. H. Youn, and B. L. Lev, Phys. Rev. Lett. **104**, 063001 (2010).
  - [19] M. Lu, N. Q. Burdick, S. H. Youn, and B. L. Lev, Phys. Rev. Lett. **107**, 190401 (2011).
  - [20] K. Aikawa, A. Frisch, M. Mark, S. Baier, A. Rietzler, R. Grimm, and F. Ferlaino, Phys. Rev. Lett. **108**, 210401 (2012).
  - [21] J. Zhang, H. Hu, X.-J. Liu, and H. Pu, Annu. Rev. Cold At. Mol. **2**, 81 (2014).
  - [22] H. Zhai, Rep. Prog. Phys. **78**, 026001 (2015).
  - [23] M. Z. Hasan and C. L. Kane, Rev. Mod. Phys. **82**, 3045 (2010).
  - [24] X.-L. Qi and S.-C. Zhang, Rev. Mod. Phys. **83**, 1057 (2011).
  - [25] J. Dalibard, F. Gerbier, G. Juzeliūnas, and P. Öhberg, Rev. Mod. Phys. **83**, 1523 (2011).
  - [26] N. Goldman, G. Juzeliūnas, P. Öhberg, and I. B. Spielman, Rep. Prog. Phys. **77**, 126401 (2014).
  - [27] J. Struck, C. Ölschläger, M. Weinberg, P. Hauke, J. Simonet, A. Eckardt, M. Lewenstein, K. Sengstock, and P. Windpassinger, Phys. Rev. Lett. **108**, 225304 (2012).
  - [28] Y.-J. Lin, K. Jiménez-García, and I. B. Spielman, Nature (London) **471**, 83 (2011).
  - [29] L. W. Cheuk, A. T. Sommer, Z. Hadzibabic, T. Yefsah, W. S. Bakr, and M. W. Zwierlein, Phys. Rev. Lett. **109**, 095302 (2012).
  - [30] P. Wang, Z.-Q. Yu, Z. Fu, J. Miao, L. Huang, S. Chai, H. Zhai, and J. Zhang, Phys. Rev. Lett. **109**, 095301 (2012).
  - [31] J.-Y. Zhang, S.-C. Ji, Z. Chen, L. Zhang, Z.-D. Du, B. Yan, G.-S. Pan, B. Zhao, Y.-J. Deng, H. Zhai, S. Chen, and J.-W. Pan, Phys. Rev. Lett. **109**, 115301 (2012).
  - [32] C. Qu, C. Hamner, M. Gong, C. Zhang, and P. Engels, Phys. Rev. A **88**, 021604 (2013).
  - [33] M. A. Khamenechi, K. Hossain, M. E. Mossman, Y. Zhang, T. Busch, M. M. Forbes, and P. Engels, Phys. Rev. Lett. **118**, 155301 (2017).
  - [34] L. Huang, Z. Meng, P. Wang, P. Peng, S.-L. Zhang,

- L. Chen, D. L. and Qi Zhou, and J. Zhang, Nat. Phys. **12**, 540 (2016).
- [35] Z. Meng, L. Huang, P. Peng, D. Li, L. Chen, Y. Xu, C. Zhang, P. Wang, and J. Zhang, Phys. Rev. Lett. **117**, 235304 (2016).
- [36] Z. Wu, L. Zhang, W. Sun, X.-T. Xu, B.-Z. Wang, S.-C. Ji, Y. Deng, S. Chen, X.-J. Liu, and J.-W. Pan, Science **354**, 83 (2016).
- [37] X. Cui, B. Lian, T.-L. Ho, B. L. Lev, and H. Zhai, Phys. Rev. A **88**, 011601 (2013).
- [38] N. Q. Burdick, Y. Tang, and B. L. Lev, Phys. Rev. X **6**, 031022 (2016).
- [39] Y. Deng, J. Cheng, H. Jing, C.-P. Sun, and S. Yi, Phys. Rev. Lett. **108**, 125301 (2012).
- [40] M. Gong, S. Tewari, and C. Zhang, Phys. Rev. Lett. **107**, 195303 (2011).
- [41] H. Hu, L. Jiang, X.-J. Liu, and H. Pu, Phys. Rev. Lett. **107**, 195304 (2011).
- [42] Z.-Q. Yu and H. Zhai, Phys. Rev. Lett. **107**, 195305 (2011).
- [43] J. P. Vyasankere, S. Zhang, and V. B. Shenoy, Phys. Rev. B **84**, 014512 (2011).
- [44] L. Han and C. A. R. Sá de Melo, Phys. Rev. A **85**, 011606 (2012).
- [45] C. Wang, C. Gao, C.-M. Jian, and H. Zhai, Phys. Rev. Lett. **105**, 160403 (2010).
- [46] T.-L. Ho and S. Zhang, Phys. Rev. Lett. **107**, 150403 (2011).
- [47] Y. Zhang, L. Mao, and C. Zhang, Phys. Rev. Lett. **108**, 035302 (2012).
- [48] Y. Li, G. I. Martone, L. P. Pitaevskii, and S. Stringari, Phys. Rev. Lett. **110**, 235302 (2013).
- [49] X. Cui, Phys. Rev. A **85**, 022705 (2012).
- [50] P. Zhang, L. Zhang, and Y. Deng, Phys. Rev. A **86**, 053608 (2012).
- [51] H. Duan, L. You, and B. Gao, Phys. Rev. A **87**, 052708 (2013).
- [52] S.-J. Wang and C. H. Greene, Phys. Rev. A **91**, 022706 (2015).
- [53] Q. Guan and D. Blume, Phys. Rev. A **94**, 022706 (2016).
- [54] Q. Guan and D. Blume, Phys. Rev. A **95**, 020702 (2017).
- [55] W. Sun, B.-Z. Wang, X.-T. Xu, C.-R. Yi, L. Zhang, Z. Wu, Y. Deng, X.-J. Liu, S. Chen, and J.-W. Pan, “Long-lived 2d spin-orbit coupled topological bose gas,” (2017), arXiv:1710.00717v1.
- [56] X. Wan, A. M. Turner, A. Vishwanath, and S. Y. Savrasov, Phys. Rev. B **83**, 205101 (2011).
- [57] A. A. Burkov and L. Balents, Phys. Rev. Lett. **107**, 127205 (2011).
- [58] With the same  $j_{\max}$ , we have also reproduced the results of Ref. [65] for dipole-dipole scattering without the presence of SOC.
- [59] J. L. Bohn, M. Cavagnero, and C. Ticknor, New J. Phys **11**, 055039 (2009).
- [60] Y. Wang and C. H. Greene, Phys. Rev. A **85**, 022704 (2012).
- [61] J. L. Bohn and D. S. Jin, Phys. Rev. A **89**, 022702 (2014).
- [62] P. Zhang and J. Jie, Phys. Rev. A **90**, 062714 (2014).
- [63] J. Wang and C. H. Greene, Phys. Rev. A **82**, 022506 (2010).
- [64] J. Wang, J. P. D’Incao, and C. H. Greene, Phys. Rev. A **84**, 052721 (2011).
- [65] K. Kanjilal and D. Blume, Phys. Rev. A **78**, 040703 (2008).
- [66] K. Aikawa, A. Frisch, M. Mark, S. Baier, R. Grimm, and F. Ferlaino, Phys. Rev. Lett. **112**, 010404 (2014).
- [67] T. N. Rescigno and C. W. McCurdy, Phys. Rev. A **62**, 032706 (2000).